

We are IntechOpen, the world's leading publisher of Open Access books Built by scientists, for scientists

6,400

Open access books available

174,000

International authors and editors

190M

Downloads

Our authors are among the

154

Countries delivered to

TOP 1%

most cited scientists

12.2%

Contributors from top 500 universities



WEB OF SCIENCE™

Selection of our books indexed in the Book Citation Index
in Web of Science™ Core Collection (BKCI)

Interested in publishing with us?
Contact book.department@intechopen.com

Numbers displayed above are based on latest data collected.
For more information visit www.intechopen.com



Chapter

Sizing and Lifecycle Assessment of Electrochemical Batteries for Electric Vehicles and Renewable Energy Storage Systems

*Arif I. Sarwat, Asadullah Khalid, Ahmed Hasnain Jalal
and Shekhar Bhansali*

Abstract

Electrochemical batteries have demonstrated quality performances in reducing emissions in Electric Vehicles (EV) and Renewable Energy Storage (RES) systems. These chemistries, although most of them commercialized, contribute to ecological toxicity and global warming in their lifecycle phases. With the addition of new energy storage chemistries, sizing uncertainty and resulting environmental damage are increasing. This chapter presents a comprehensive comparative exploration of 14 electrochemical batteries, including chemistries in the research and development phase. To identify the appropriate chemistry, the capacity range sizing criteria, and formulations are presented with case studies of Environmental Protection Agency (EPA) approved driving profiles for EVs, and consumption load profiles for RES systems, dependent on a given set of operational constraints. Furthermore, a lifecycle impact assessment (LCA) metric, the Cradle-to-Gate technique, is computed to evaluate the sized storage chemistries' environmental impact supported by five case studies considering short-, medium-, and long-term duration operations and storage services.

Keywords: electric vehicles, renewable energy storage systems, electrochemistry, lifecycle assessment, cradle-to-gate, battery sizing

1. Introduction

Solar photovoltaics and wind turbines have been the least expensive ways to generate electricity, however, with the increased maintenance requirements in these systems, the demand is shifting and growing towards maintenance-free electrochemical batteries [1]. This has resulted in the development of a wide variety of secondary storage battery chemistries and this demand increase is further supported by the decrease in their prices. For instance, the Lithium-ion (Li-ion) battery, which was once one of the most expensive chemistries with prices over \$450/kWh has seen a

reduction in per-kWh prices to as low as \$200. Berckmans et al. [2] predicts the price to drop down further to less than \$150/kWh (by 2030). In order to reduce greenhouse emissions from vehicles as well as firm renewables for smart city development, a cut above storage chemistry is needed [3]. Lifecycle (impact) assessment (LCA) is a metric to evaluate the equivalent emissions and the damage an energy storage system does to the environment. As defined in ISO 14040 and 14,044, the parameters required for LCA analysis include functional unit, system boundary, impact category, and a data source. Commonly used data sources include E.U. Ecoinvent database, and U.S. GREET. Using Argonne National Laboratory's BatPaC (Battery Performance and Cost) Model. Greenhouse gas emission (GHG), Human health (HH), Ecosystem quality (EQ), Resources depletion (RD), Cumulative water use (CWU), Global warming potential (GWP), Ecotoxicity (ET), Acidification (AD), Ozone depletion (OD), Photochemical smog (PS), Eutrophication (EP), and Cumulative energy demand (CED) are the commonly used impact categories for LCA analysis in literature.

Cradle-to-gate is a standard development period that is taken as the assessment term in this study. Cradle-to-gate along with use impact is also associated and sometimes proportional to the greenhouse gas emissions, which makes it an important evaluation factor for the application-specific storage chemistry assessment [4–9]. CED is a metric to identify the environmental burden (or the lifecycle impact) imposed by a commodity's production and/or its use. This metric, in MJ/kWh, would be used to evaluate the Cradle-to-gate with use impact of selected chemistries.

A technology readiness level chart of all 14 EV and RES (galvanic) electrochemical batteries discussed in this paper is shown in **Figure 1**. This gives an idea of the chemistries which had the potential of going through numerous research and development iterations. For instance, the Lead Acid (Pb-Acid) chemistry has had over 160 years since its discovery in 1859 to go through ameliorations. Charge holding capacity, time duration, and degradation abridging potential are the crucial appraising factors that have been improved upon for every other storage chemistry that is currently commercialized [10, 11]. Further study on improvement and discussions of these key topics are presented in the following sections. Section 2 discusses the electrochemical redox performance of these 14 chemistries and suggests the applicable upside and downside to their designs and developments. Section 3 provides mathematical formulations and results for sizing a battery, taking into consideration a case study of a 2000Kg EV as well as another case study of a hospital and a primary school's loads in Miami, Florida. Section 4 presents the Cradle-to-gate model for LCA of the sized battery chemistries for the EV, hospital, and primary school taking into consideration their electrochemical performance values as well. Section 5 concludes the paper with a scope for future work.

The key contributions of the paper are that it: (1) Provides a comprehensive technical categorization of batteries based on their electro-chemistry; (2) Provides energy storage sizing criteria and formulations for EV and RES systems; (3) Evaluates chemistry- and application-specific lifecycle performance of EV and RES batteries using cradle-to-gate method based formulations.

2. Battery electrochemistry performances evaluation

Specifications comparison is a major preliminary requirement for a battery to be implemented for any defined application [12]. This section discusses the performance,

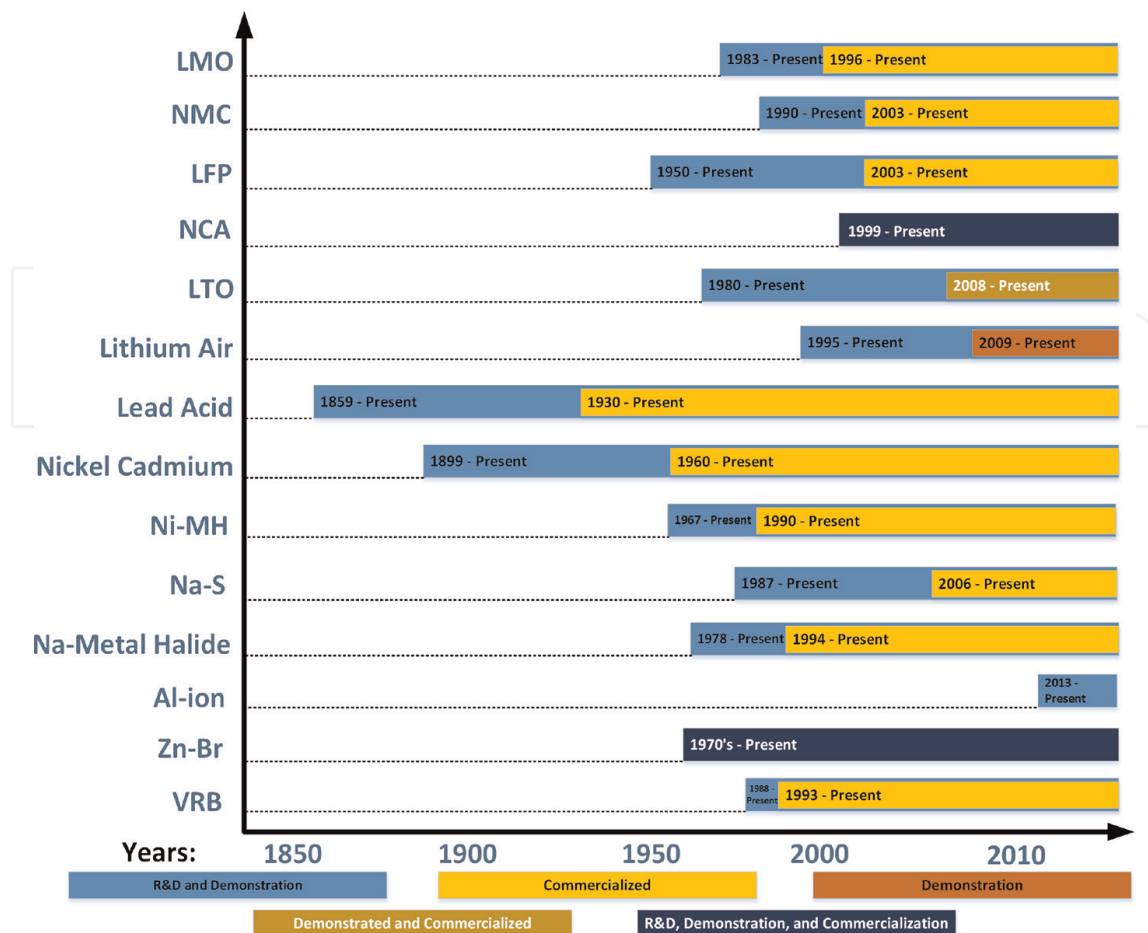


Figure 1.
 Technology readiness levels of EV and RES electrochemical batteries.

internal electrochemical phenomenon details, and redox reactions of the 14 EV and RES chemistries analyzed in **Figure 1**. The effect of Depth-of-Discharge (DOD%) on separate chemistries is also studied in this section, which is an important factor for the case studies discussed in Section 4.

2.1 Lithium based batteries

Lithium is a highly researched cell chemistry because of its high specific energy, high cycle life, low self-discharge, and high nominal voltage [13–20]. It supersedes other chemistries such as Lead-acid, Nickel Cadmium (Ni-Cd), and Nickel Metal Hydride (Ni-MH) in almost every category except in over charge and over discharge situations [21]. This sub-section compares and evaluates various commercially available and under development Li-ion chemistries used in EVs and RES systems. Common Lithium chemistries categorized by their properties, composition, along with their possible uses are listed in **Table 1**.

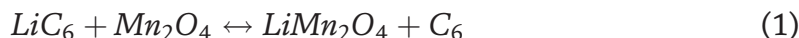
Lithium Manganese Oxide (LMO or $LiMn_2O_4$) has a spinel structure with a nominal voltage of 3.8 V (Eq. 1) [43, 44]. Its low cost and high thermal stability are attributable to the addition of Manganese. Manganese is cheap and low in toxicity, but does not have a high specific energy. This has led to the development of the Lithium Nickel Manganese Cobalt Oxide (NMC or $LiNiMnCoO_2$) chemistry. NMC type lithium cells are created through the addition of Nickel [43, 44]. Nickel, on its own,

	Lithium Manganese Oxide (LMO) [22–28]	Lithium Nickel Manganese Cobalt Oxide (NMC) [22, 23, 25, 27, 29–31]	Lithium Iron Phosphate (LFP) [22, 23, 25, 27, 30, 32, 33]	Lithium Nickel Cobalt Aluminum Oxide (NCA) [22, 23, 25, 27, 30, 34]	Lithium Titanate (LTO) [22, 23, 25, 26, 31, 35, 36]	Lithium Air (LiO_2) [37–40]
Anode	Graphite	Graphite	Graphite	Graphite	LTO	Lithium
Cathode	Lithium Nickel Manganese Spinel	NMC	LFP	NCA	LMO or NMC	Porous Air
Electrolyte	$LiPF_6$ in organic solution [†]	$LiPF_6$ in organic solution [†]	$LiPF_6$ in organic solution [†]	$LiPF_6$ in organic solution [†]	$LiPF_6$ in organic solution [†]	Hybrid*
Specific Energy (Wh/Kg)	100–150	150–220	90–120	~ 280	50–80	5200*
Specific Power (W/Kg)	110–340	110–340	200–1200	110–340	3000–5100	0.46*
Safety (Thermal Stability)	++	+	+++	—	+++	++
Nominal voltage	3.8 V	3.6 V	3.3 V	3.6 V	2.2 V	2.9 V
Charging voltage	4.2 V	4.2 V	3.6 V	4.2 V	2.8 V	3.3 V
Cycle Life	300–700	2000–6000	2000–2010,000	500–1000	3000–7000	~ 2000*
Discharge curve	Flat	Sloping	Flat	Sloping	Sloping	Flat
Cost (\$/kWh)	Low	Medium	Low	High	Very High	N/A*
Applications	EV, HEV, PHEV, RES	EV, HEV, PHEV, RES	EV, HEV, PHEV, RES	EV, HEV, PHEV, UPS, RES	HEV, RES	Aviation*, EV*
Form Factor	Coin, Cylindrical, Prismatic, Pouch	Cylindrical, Prismatic, Pouch	Cylindrical, Prismatic, Pouch	Cylindrical, Prismatic, Pouch	Cylindrical, Prismatic, Pouch	N/A*
Technology Readiness Level	R&D, Dem., Com.	R&D, Dem., Com.	R&D, Dem., Com.	R&D, Dem., Com.	R&D, Dem., Com.	R&D

Labels: Poor (–), Good (+), Very Good (++), Excellent (+++).
 RES: Renewable Energy Storage; EV: Electric Vehicles; HEV: Hybrid Electric Vehicles; R&D: Research and Development; Dem.: Demonstration Stage; Com.: Commercialized.
 *as per [41, 42], still undergoing R&D.
[†]Manufacturer dependent. Standard organic solution is ethylene carbonate (EC)–dimethyl carbonate (DMC) mixture.

Table 1.
Lithium based batteries comparison based on their electro-chemistries.

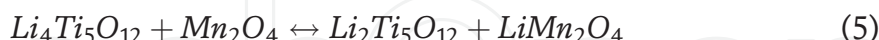
provides high energy density but lower thermal stability, therefore Manganese is added to create a more stable chemistry (in NMC) that increases cycle life and stability (Eq. 2) [45].



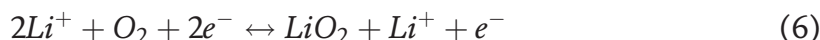
Lithium Iron Phosphate (LFP or $LiFePO_4$) batteries, on the other hand, have improved safety and thermal stability due to the addition of Iron that creates the olivine structure (Eq. 3) [43, 44]. Subsequently, these cells can operate at higher temperatures effectively, however, their specific energy tends to be lower than that of other lithium chemistries, especially Nickel Cobalt Aluminum Oxide (NCA or $LiNiCoAlO_2$) [45, 46]. NCA has a high specific energy and lower thermal stability, both owing to the addition of Nickel [45, 47]. Aluminum present in NCA creates a similar layered crystal structure like in NMC (Eq. 4) [43, 44]. Comparison between LFP, NMC, and NCA in [48] showed that an increasing SOC % increases the temperature of LFP by around $0.8^\circ C$ per SOC value. The corresponding values for NMC and NCA increase by $1.02^\circ C$, and $1.74^\circ C$ per SOC % respectively. The NCA lithium battery has twice the potential to catch fire if overcharged, when compared to LFP. This further emphasizes the importance in selection of correct lithium chemistries and in general, an effective battery management system for EV and RES applications.



Lithium Titanate (LTO or $Li_4Ti_2O_{12}$) has a low specific energy and high cost (Eq. 5) [43]. In addition, its nominal voltage is very low. An EV or RES manufacturer would need to practically double the number of cells in series to reach the same voltage as the NMC/NCA/LMO chemistries. This will greatly increase the cost and weight of the vehicle and decrease the amount of usable space. These batteries also contain a unique anode composed of LTO which drastically increases its thermal stability and cycle life when compared to other Lithium chemistries. The improved safety/lifespan of LTO can be attributed to the limited expansion of the anode (only 0.2% of volume changes) during charge/discharge operation [45].



Combination of phenomena of Lithium oxidation at the anode, and oxygen reduction at the cathode, using electrolytes ranging from solid state, to aqueous, non-aqueous, or aprotic solvent variants, results in the formation of the Lithium Air (LiO_2) battery. This anode and cathode pair creates a practical specific energy of 18.7 MJ/Kg , which is about 10–15 times higher than that of a commercially available Li-ion battery [49]. Oxygen molecules entering cathode through the porous cathode react with Li^+ ions moving from the anode via an electrolyte, to form Lithium Peroxide (Li_2O_2) while the electrons flow through the external load during a discharge operation, constituting the redox reaction shown in Eq. (6).



LiO_2 batteries can operate effectively at temperatures up to $140^\circ C$ [50]. They are still under development mainly due to their varying performances with changing electrolytes. LiO_2 started off as an accidental discovery by K. M. Abraham in 1995 while using a non-aqueous electrolyte [51] however deposition of Li_2O_2 on the cathode

electrode with time called for more exploratory research. Liu et al. [52] in 2015 proposed the addition of lithium iodide and water to make the electrodes spongy along with a hybrid (combination of solid state and aqueous) electrolyte, thereby resulting in Lithium Hydroxide crystals which do not coat the surface and impede the flow of electrons, allowing continuous voltage supply. Although this research improves the operational lifetime of the battery, it reduces the overall specific energy due to the inclusion of water.

NCA, LTO, and NMC have sloping discharge curves while LMO, LFP, and LiO_2 have flat discharge curves (**Table 1**). Understanding charge/discharge characteristics of each chemistry is important when selecting a cell to be tested for an application. Generally, the sloping discharge curve reduces the complexity in model selection since the voltage level decreases almost proportionally with SOC%.

The ease with which the electrochemical reaction will occur depends on the ionic/electrical conductivities. Lower conductivities will result in greater resistance and lower efficiency in the conversion from chemical to electrical energy. These values heavily depend on the central testing conditions [17]. Furthermore, for the electrolyte, the ionic conductivity is an important consideration with high conductivity being ideal. During charge and discharge cycles, Lithium ions are shuttled across the electrolyte to the anode and cathode, respectively. Decreased resistance from Lithium ions traversing from anode to cathode and vice versa will mean less heat generation and increased efficiency of the cell [53–56].

Every Lithium chemistry eventually degrades over time from a variety of factors. Solid electrolyte interphase (SEI) development is one of the main contributing factors to degradation. The formation of this layer is important because it allows Li-ion transportation but prevents electrons from moving through resulting in further decomposition of the electrolyte [57].

In addition to charging or discharging operations, factors like storage and thermal conditions also play a major role in SEI formation. The authors in [58] show that the capacity of batteries being stored drastically declines with the increase in temperature. Lithium batteries have a good shelf life but are still prone to losing capacity if stored for an extended period. Increased depth of discharge (DOD) also decreases the cycle life of the cell. Data from [59] shows that discharging the cell too deeply will greatly impact its capacity after many cycles. After 25,000 cycles, a cell discharged at a consistent 30% DOD lost 53% of its capacity, while a cell discharged at 20% DOD lost 40% percent of its capacity with both being at 20°C. Based on these findings, it can be concluded that DOD has a substantial effect on the cycle life of a Lithium-ion battery. Moreover, a decrease in the cell's capacity over many cycles caused by the aforementioned conditions leads to internal issues that are reflected in the cell's available capacity. Some examples are Lithium plating at the anode from high charge current, SEI formation on the anode from electrolyte decomposition due to high temperature/DoD, and volume changes on the anode and cathode due to all of the above stated conditions [60]. Other additional comparative features of the discussed Lithium based chemistries are tabulated in **Table 1**.

2.2 Pb-acid based batteries

Physicist Gaston Plante invented the Pb-acid based battery, which is comprised of lead dioxide (PbO_2) as the anode, lead (Pb) plate as the cathode, and aqueous sulfuric acid (H_2SO_4) as the electrolyte. The reaction mechanism of these batteries relies on

oxidation (on the anode) and reduction (on cathode) reactions and follows the redox reaction shown in Eq. (7):



The electrical turnaround efficiency of these batteries is 75–80% with specific energy ranging between 30 and 50 Wh/kg [61], which is much lower than other EV or RES battery chemistries. Also, the cycle life of these batteries is comparatively short (< 2000 cycles) [62]. Sulfation is one of the major causes of this lower cycle life, which impedes recharging and causes cracking into the electrode plate [63]. This incident causes inadequate charging during regular operation due to amorphous lead sulfate deposits on the negative electrode, which turns into a crystalline structure in a progression. Consequently, the active materials of the negative electrode are covered with this additional layer. This issue can be resolved by integrating the high content of carbon into the lead electrode, which promotes the self-recharging rate and cycle life [63]. The formation of the carbon-Pb alloy accelerates water loss and inner pressure due to the hydrogen evolution reaction [64, 65]. This reaction mechanism involves either absorption or desorption of the intermediate hydrogen by the electrode surface in two separate routes termed as the Volmer-Tafel and Volmer-Heyrovsky mechanisms [66, 67]. The activated carbon doped with heteroatoms (e.g., N, P, B, or S) in the graphene ring improve the charge acceptance and charge retention ability of the Pb-acid based battery and inhibits the hydrogen evolution reaction. Also, Pb-acid requires an additional mandatory thermal management system for reliable temperature efficiency. Moreover, they are bulky in weight, require prolonged charging time and cyclic water maintenance, and suffer from premature failure and degradation at high power operation. However, on the upside, these batteries are cost-effective (in manufacturing and maintenance) and easily recyclable ($\geq 97\%$ recycling efficiency) [68]. Additionally, their charge retention capability is compatible with both grid and automotive applications. For obtaining the required power/energy ratings, an array of Pb-acid battery cells are connected in such a way that each cell voltage and range of charging rate are 2.15 V and 0.25–4, respectively [69]. Pb-acid batteries are mostly employed as a backup power supply in the range of kW to tens of MW for grid utilities and hybrid electric vehicles. All the comparative features of this chemistry are tabulated in **Table 2**.

2.3 Ni-based batteries

Ni-based batteries are classified into two broad categories: Ni-Cd based batteries, and Ni-MH based batteries. Generally, nickel oxyhydroxide is used as the anode, and Cd or MH, are employed as the cathode. The electrolyte is an aqueous alkaline solution, such as aqueous potassium hydroxide (KOH), used for both Ni-MH and Ni-Cd based batteries. Zn, Fe, or H_2 -based Ni batteries are also used in the applications tabulated in **Table 2**.

Compared with Ni-Cd or Ni-MH based batteries, these Ni-based chemistries have limitations in terms of energy density (low), efficiency (low), maintenance cost (high), lifecycle (low), and self-discharging issues [92]. Contrarily, Ni-Cd performs with 70–90% efficiency, has moderate energy density (50–75 Wh/kg), higher lifecycles (2000–2500), a 10%/month self-discharging rate, and better temperature tolerances [69, 93, 94]. However, both the Cd and Ni chemistries are considered as hazardous substances, and the manufacturing costs of Ni-Cd batteries are also

	Pb-Acid [12, 64, 70, 71]	Ni-Cd [12, 70, 71]	Ni-MH [12, 70, 71]	Na-S [71–75]	Na Metal Halide [76–80]	Al-ion [81–85]	Zn-Br [12, 86–90]	VRB [12, 91]
Anode	PbO ₂	NiOOH	NiOOH	Na	Na	Al	Carbon Polymer Composites	Carbon Polymer Composites
Cathode	Pb-plate	Cd	Metal Hydrides	S	Porous Transition Metal	Graphite	Carbon Polymer Composites	Carbon Polymer Composites
Electrolyte	Aqueous H ₂ SO ₄	KOH	KOH	β – Al ₂ O ₃	β – Al ₂ O ₃	1-ethyl-3methylimid- azolium chloride*	Zinc Bromide	Vanadium Pentoxide + Sulfuric Acid
Specific Energy (Wh/Kg)	30–50	50–75	40–110	150–240	120–240	40*	75–85	35
Specific Power (W/Kg)	180	150–300	250–1000	90–230	150–230	3000*	90–110	805
Safety (Thermal Stability)	+	+	+	—	+	++	++	++
Nominal voltage /OCP	2 V	1.2 V	1.2 V	2–2.5 V	2.58 V (Ni), 2.33 V (Fe)	2 V*	1.8–1.85 V	1.15 V
Charging voltage	2.15 V	1.55 V	1.6 V	2.67 V	2.67–2.85 V	0.5–2.45 V*	2 V*	1.6 V
Cycle Life	< 2000	2000 to 5000	~ 3000	2500–4500	300–500	7500*	> 2000	12,000–20,000
Discharge curve	Flat	Flat	Flat	Sloping	Flat	Variable*	Flat	Sloping
Cost (\$/kWh)	Low	Medium	Very High	Medium	High	N/A*	Medium	Low
Applications	RES, EV, Industrial	Military, Aviation, EV, RES	RES, EV	RES	RES, EV, HEV, Railways	RES	RES, EV*	RES
Form Factor	Coin, Cylindrical, Prismatic, Pouch	Coin, Cylindrical, Prismatic, Pouch	Coin, Cylindrical, Prismatic, Pouch	Cylindrical	Cylindrical, Prismatic	N/A*	Tank Storage	Tank Storage
Technology Readiness Level	R&D, Dem., Com.	R&D, Dem., Com.	R&D, Dem., Com.	R&D, Dem.	R&D, Dem., Com.	R&D	R&D, Dem., Com.	R&D, Dem., Com.

Labels: Poor(–), Good (+), Very Good (++)
RES: Renewable Energy Storage; EV: Electric Vehicles; HEV: Hybrid Electric Vehicles; R&D: Research and Development; Dem.: Demonstration Stage; Com.: Commercialized.
*Still undergoing R&D.

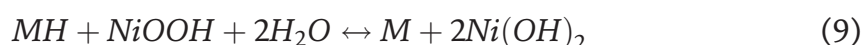
Table 2.

Pb, Ni, Na, Al-based and redox batteries comparison based on their electro-chemistries.

relatively high (\$1000/kWh and ten times higher than Pb-acid based batteries). The electrodes, electrolyte, and separator (insulator between anode and cathode) are placed in a low cost and flame-retardant polymer (e.g., polypropylene, polystyrene) container for these batteries. The redox reaction for Ni-Cd based batteries is shown by Eq. (8).



Ni-MH batteries are the other category which is commercially established for the uninterrupted power supply in different applications, such as grid systems, hybrid electric vehicles, and communication systems. Different metal hydrides and Nickel hydroxide (NiOOH) are employed as the anode and cathode, respectively [73]. The overall charging and discharging reaction mechanism in Ni-MH based batteries follows Eq. (9):



Both the anode and cathode are porous in structure. Therefore, they have a large surface area, which enhances the rate of reaction and internal conductivity. Hence, their energy density (40–110 Wh/kg) is higher than Ni-Cd based batteries. Additionally, this battery system is environmentally benign, has high charging and discharging tolerance, longer shelf, cycle life (~3000 cycles) and can operate in a wide temperature range (30–70°C). However, both above-mentioned Ni-based chemistries suffer from the “memory effect”, which happens due to incomplete discharges in preceding uses. Consequently, the energy capacity and rated output potential abruptly deteriorate leading to another effect termed as the “voltage depression effect” [95]. However, this effect can be mitigated by proper charging-discharging management of the battery systems. All the comparative features of both of these chemistries are also tabulated in **Table 2**.

2.4 Na-β based batteries

Following chemical composition and reaction mechanisms, Na-β based batteries are classified into the following two types: Sodium-sulfur (Na-S) and sodium-metal halide. A tubular-shaped beta-alumina (βAl_2O_3) ceramic is employed as an electrolyte, which acts as a superionic conductor and a separator (between the anode and cathode) simultaneously. All these materials are naturally abundant and inexpensive. In Na-S based batteries, both the cathode (S) and anode (Na) are in molten form. Due to oxidation, Na^+ ions are generated at the cathode, which are carried by the β-alumina based solid electrolyte. Later, these ions recombine at the anode and vice versa for the reduction reaction. The overall redox reaction for this chemistry is shown in Eq. (10).



Their energy density and self-discharging rate fall in the range of 140–240 Wh/kg and 1% respectively [96, 97]. Additionally, these batteries have a short response time (1 ms), higher energy efficiency (75–90%), and good recyclability (99%) [69]. At 100% DOD, their lifecycle is around 2500, whereas it increases to 4500 by dropping DOD to 80% [97]. Moreover, this battery system has shown efficient results and is capable of voltage stability (short duration), peak shaving (medium duration), and

load leveling (long duration) grid service requests. These batteries operate at 300–350°C in a thermal enclosure and have a significant tolerance for running in both cold and hot temperatures. However, the operation in a high temperature promotes corrosion and explosion. Hence, this battery system requires a mandatory thermal management system. In September 2011, a 2000 kW – NaS-based battery system from NGK, consisting of 40 battery modules, exploded at Tsukuba in Japan [98]. Another fire incident occurred in a 30-megawatt Kahuku wind farm in Hawaii [99]. Apart from reasons related to other interconnected components, the main reason on the battery side was that one of the faulty cells was ignited by inundating the molten materials over the filler portion of the blocks and was causing a short between the cells.

The other sodium-based chemistry, Sodium metal halide ($Na - MeCl_2$) is another alternative and promising battery for the next generation stationary energy storage systems. They have compatible features, which include reliability, resiliency, and higher roundtrip efficiency. The anode and electrolyte of this battery is similar to the Na-S based batteries. However, the cathode is made from a porous transition metal (Ni or Fe) halide matrix infused by an additional secondary electrolyte, sodium tetrachloro-aluminate ($NaAlCl_4$). This inorganic electrolyte provides higher ionic conductivity and superior battery safety [100]. The transport mechanism of the Na^+ ions through $\beta-Al_2O_3$ and $NaAlCl_4$ are reversible for the charging-discharging processes. The reaction mechanism between pyrophoric metal (Na) and hygroscopic metal halides is as shown in Eq. (11), where ‘Me’ stands for Ni or Fe metals.



The theoretical specific energies for Ni and Fe are as high as 788 Wh/kg and 729 Wh/kg respectively. However, the energy density of these batteries lies between 120 and 240 Wh/kg [100, 101]. These batteries can operate over 20 kWh which indicates that they are strong candidates for EV and RES applications. There is no self-discharge (that is, a coulombic efficiency of 100%) occurrence in this battery, and their cycle life is over 1000 at 100% DOD. Additionally, these batteries are corrosion-protective and can operate in the lower resistive cell-failure mode with better charging/discharging tolerance, which ensures higher safety than that of the Na-S battery system. However, their high manufacturing cost, intricate cell architecture, high operating temperature (300–350°C), and performance deterioration with cycling are still a constraint [102, 103]. The high operating temperature is the cause of the high corrosion rate. A high-cost hermetic sealing is essential in this system to prevent this corrosion of the materials and degradation of the performances at high temperatures. All of the comparative features of this chemistry are also tabulated in **Table 2**.

2.5 Aluminum-ion (Al-ion) batteries

In the past few years, Al-ion batteries are considered as one of the promising categories of rechargeable batteries for electric vehicles, renewable energy, and mobile devices. Aluminum, being an abundant material, makes these batteries reasonably accessible with low price in comparison with Li-ion batteries (Lithium is only 0.0065 wt% of the earth’s crust) [82, 104, 105]. Lin et al. (Dai group) from Stanford University reported the first paper on such kind of batteries, which consist of aluminum as the anode, an aqueous ionic electrolyte from vacuum dried $AlCl_3$ /1-ethyl-3-methylimidazolium chloride, and graphite as the cathode [83]. The charging and

discharging mechanisms of these batteries rely on the electrochemical deposition/dissolution of Al at the anodic electrode and the intercalation/deintercalation of chlor-aluminate ions ($AlCl_4^-$) in the cathodic electrode based on the reactions shown in Eq. (12) and (13).



The nominal voltage obtained from this reaction is around 2 V, and the coulombic efficiency was as high as 98% [105]. These batteries can maintain their lifecycle at around 7500 without compromising significant power density (specific power). Their maximum specific energy and power were obtained to be 3000 Wh/kg and 40 Wh/kg respectively [83]. Moreover, they have a superior recharging ability (1.1 – 60s, with a specific capacity in the range of 60–110 mAh/g) due to their active electrode kinetics and reduced polarization effect. This chemistry is new and still in the research phase. All the comparative features of this chemistry are also tabulated in **Table 2**.

2.6 Flow batteries

In Vanadium Redox batteries (VRB), Vanadium-anolyte and –catholyte half cells are stored in electrolyte tanks which allow flow through the adjacent half cells and are separated by an ion exchange membrane. During the charge process, Vanadium ions catholyte half-cell, V^{3+} are converted into V^{2+} resulting in an electron attracted by the positive electrode (cathode) and hydronium (H^+) which diffuses into the anode half-cell via the membrane. At the anolyte half-cell, the electron from the cathode (via the external load) converts existing VO_2^+ in anode to VO^{2+} thereby balancing (with H^+ ion) and storing the chemical energy. During discharge process, the stored chemicals start feeding the external load. During this process, the VO_2^+ ion is oxidized to VO^{2+} releasing the hydronium ion and the process continues until the anode contains V^{3+} ion and is completely discharged. The applicable redox reaction is shown in Eq. (14) [106].



Although VRB's have long cycle life and high energy efficiency, they constitute only 30% of the energy storage market share [107]. This is mainly because of its limitations which include high form factor, low volumetric energy storage capacity, expensive ion exchange membrane, and low specific energy in comparison to Li-ion, which constitutes 60% of market share [108].

Another redox flow chemistry used in renewable energy storage, Zinc bromine (Zn-Br) batteries, categorized as hybrid redox flow batteries, include carbon-polymer composites as electrodes isolated by microporous polyolefin membrane (separator). One of these electrodes is submerged into the aqueous solution of zinc bromide as the anolyte. The catholyte comprises of two aqueous phases: a solution of Zn-Br at the top layer and dense bromine in the form of a complex organic solution at the bottom [109]. Aqueous zinc bromide is converted into metallic zinc through the electrolyzation process during charging, and the zinc bromide salt is altered back from Zn and bromine during the discharging process. The applicable redox reaction is shown in Eq. (15).



The bromine is expelled during this process and is poisonous, highly oxidative, and less soluble in water. Hence, an additional compound, organic amine, is added to dissolve it in the solution as viscous bromine adduct oil. Additionally, Zn also tends to deposit on the electrode during charging in the form of a dendrite crystal structure with a high current density, which may cause short circuits through the polyolefin membrane [110]. The surface morphology of this electroplated Zn is determined by the current density, temperature of the solution, and the flow velocity [111]. Hence, the overall capacity of energy storage in this battery system relies on the electrolyzation process and the surface area of the electrode, that is, the stacks size and the volume of the electrolyte storage reservoirs. Therefore, the energy ratings of these batteries are not entirely distinct. This battery system requires an obligatory temperature (below 50°C) and oxidation control system for safety, which makes it expensive [112]. The energy density (75–85 Wh/kg), efficiency (65–75%), and cycle life (>2000 cycles) of this battery vary within a moderate range [113]. Some significant advantages of these batteries are their flexibility in ambient-temperature operation, compatible power density in RES and EV applications, fast charging capability, and 100% DOD without any damage to the battery system [11, 89]. All of the comparative features of both of these chemistries are also tabulated in **Table 2**.

3. Stationary and In-motion energy storage systems application-specific sizing

3.1 Electric vehicle storage application-specific sizing

Due to widespread use of EVs, standards and regulations have been developed by various regulatory bodies [114]. These regulations include EPA certified driving patterns which permit the minimum permissible operational boundaries for an EV [115]. Four such EPA certified driving patterns are used as the criterion for EV storage sizing in this section. The Federal Test Procedure (FTP) version 75 defined by EPA as a test cycle for emission certification of light duty vehicles is a mandatory test procedure designed to identify the fuel economy performance of new vehicles. It consists of complex driving phases including a cold start phase until 505 seconds, a stabilized phase between 506 and 1375 seconds, and a hot start phase from 1376-1874 seconds. This test represents a transient driving cycle with an average speed of 9.47 meter/second (21.2 miles/hour). The second profile, the Highway Fuel Economy Driving Schedule (HWFET) test cycle, defines certification and performance requirements for driving conditions on a highway. The average speed in this cycle is 21.59 meter/second (48.3 miles per hour). The third profile, the New York City Cycle (NYCC) test cycle, defines stop-and-go traffic driving constraints to assess the vehicle. The average speed in this cycle is 21.62 meter/second (48.37 miles per hour).

For EV certification applications, each of these tests assess vehicle performance, battery state, and energy consumption to simulate the vehicle model prior to production. The velocity versus time plots of each cycle (plotted in **Figure 2** and data for which is obtained from [116]) represent how a vehicle travels under different terrains and conditions, satisfying the minimum EPA requirements.

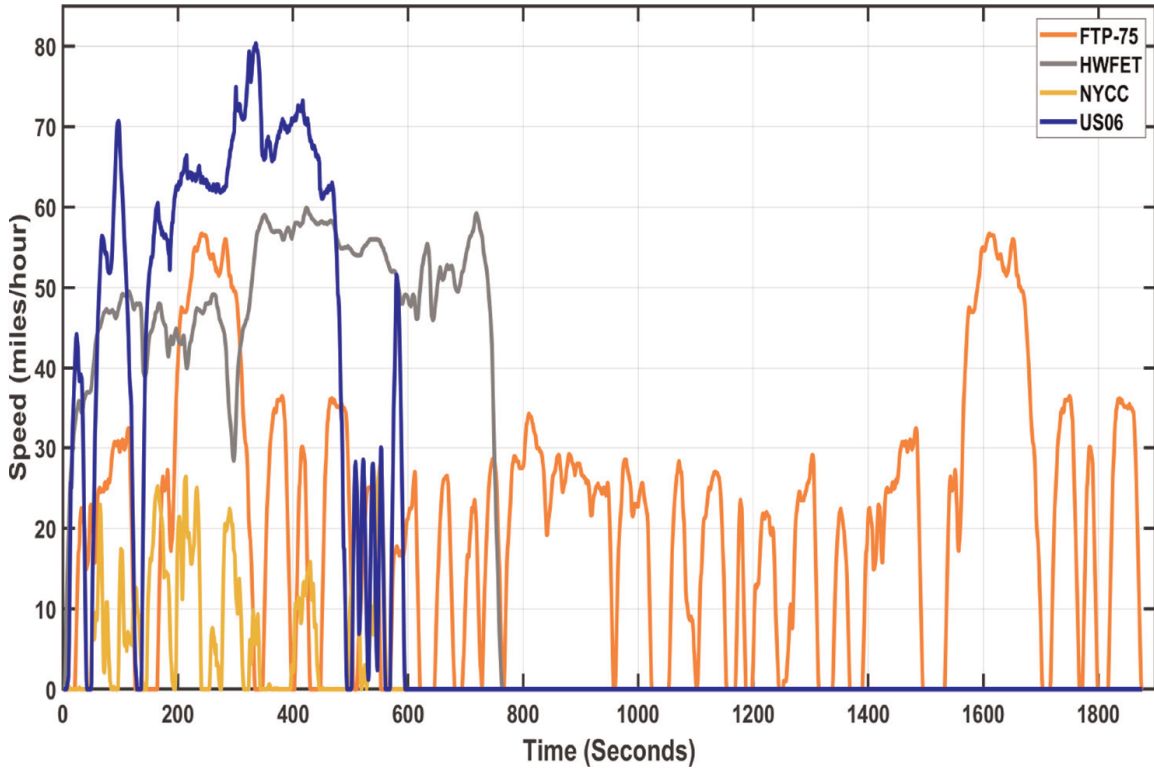


Figure 2.
 Standard EPA driving profile plots.

Table 3 shows a sizing case study listing applicable values for a 2000 Kg (4409 lbs) EV. The set of equations used for computing the minimum and maximum battery capacity for the EV are shown in Eq. (16).

$$E_{max(or\ min)} = P_b * \delta_{max(or\ min)},$$

$$P_b = \frac{\text{Power required by wheels}}{\eta_t * \eta_d} + \frac{P_{acc}}{\eta_a},$$

$$\text{Power required by wheels} = 9.8 * V(r_t + r_w + r_g + 1.1 * r_a),$$

$$r_t = \frac{w}{65} * (1 + 4.68 * 10^{-3} * V + 1.3 * 10^{-4} * V^2), \quad (16)$$

$$r_w = \frac{\rho_a}{g} * \frac{V^2}{2} * (C_d * \lambda),$$

$$r_g = w * \text{Sin}\theta,$$

$$r_a = \frac{w}{g} * \frac{d(V)}{dt},$$

where, gravitational acceleration (g) = $9.8\ m/s^2$, and air density (ρ_a) = $1.225\ Kg/m^3$. Weight of the battery is generally $\leq 30\%$ of vehicle weight. In this case, the velocity averages are identified from the above-mentioned standard driving cycles. The velocity differentials are calculated by building the linear trend-line equations for each of the driving cycles, as shown in Eq. (17). The parameters: θ , C_d , λ , η_a , η_d , η_t , and P_{acc} values are assumed averages from currently commercialized vehicles' testing

w	V	θ	C_d	λ	η_a	η_d	η_t	P_c	$\frac{d(V)}{dt}$	r_a	r_g	r_w	r_t	P_b	δ range	E_{min}	E_{max}
FTP-75 Driving Cycle																	
20	9.47	2	0.2	0.8	0.9	0.9	0.9	6	0.0002	-7.4	1826	1.1	32.4	181.46	0.03-0.5	5.4	91.13
HWFET Driving Cycle																	
20	21.59	2	0.2	0.8	0.9	0.9	0.9	6	0.0166	-7.4	1826	5.7	35.7	415.31	0.03-0.5	12.5	209
NYCC Driving Cycle																	
20	3.17	2	0.2	0.8	0.9	0.9	0.9	6	0.0007	-7.4	1826	0.1	31.2	60.7	0.03-0.5	1.8	30.49
US06 Driving Cycle																	
20	21.62	2	0.2	0.8	0.9	0.9	0.9	6	-0.069	-0.4	1826	5.8	35.7	415.89	0.03-0.5	12.4	207.12

w : EV Gross Weight (in kg); V : Average Driving Cycle Velocity (in m/s); θ : Angle of Inclination of the Terrain; C_d : Air Drag Coefficient; λ : Frontal Area of Vehicles (in m^2); η_a : Electrical Efficiency of Accessories; η_d : Electrical Efficiency of Drive-train; η_t : Mechanical Efficiency of Transmission; P_{acc} : Power required by accessories (in Watts); r_a : Acceleration Resistance (in Newtons); r_g : Gravitational Resistance (in Newtons); r_w : Wind Resistance (in Newtons); r_t : Rolling Resistance of tires (in Newtons); P_b : Battery Power (in kW); δ range: Common $\frac{\text{Specific Energy}}{\text{Specific Power}}$ ratio range of commercialized batteries; E_{min} : Minimum Battery Capacity (in kWh); E_{max} : Maximum Battery Capacity (in kWh).

Table 3.
Battery storage capacity range identification using driving cycles, for a 2000 kg (4409 lbs) vehicle.

specifications where variations in these values do not create a major change in the resulting battery capacity size. The key parameter is w , in which a minor change largely varies the battery capacity size range for the respective driving schedules.

$$\begin{aligned} \text{FTP} - 75 : V &= 0.0002t + 20.995, \\ \text{HWFET} : V &= 0.0166t + 42.052, \\ \text{NYCC} : V &= 0.0007t + 7.3611, \\ \text{US06} : V &= -0.0069t + 50.594 \end{aligned} \tag{17}$$

The resulting average energy (battery capacity) is 105 kWh, that is the average of the lowest (1.83 kWh) and the highest (207.12 kWh) values. In terms of current commercially available and EPA certified vehicles, a 2020 Nissan Leaf (3946 lbs., 62 kWh), or a 2012 Tesla Model S (4,323 lbs., 100kWh) fall within this weight - battery capacity range combination.

3.2 Renewable energy storage application-specific sizing

The electricity load profile analysis method termed as load summation method is used for computing the RES battery based on average and peak load calculations [117, 118]. In the average load calculation method, the average of the sum of hourly consumptions of the facility is taken into consideration which is mainly performed to define sizes for storage systems used for contingency planning or for operating limited-power (set of) equipment. The peak load calculation uses the peak of hourly consumptions of the facility to design a storage system which is capable of operating all the equipment for a defined period of time. In this case, hourly load profiles of a primary school and a hospital, both located in Miami, Florida for the year 2004 is obtained from [119, 120], corresponding plots for which are shown in **Figures 3** and **4** respectively.

The reason for the selection of the two datasets is the extremity in load profile variations and the frequency of variations. The sizing equations used for the analyses

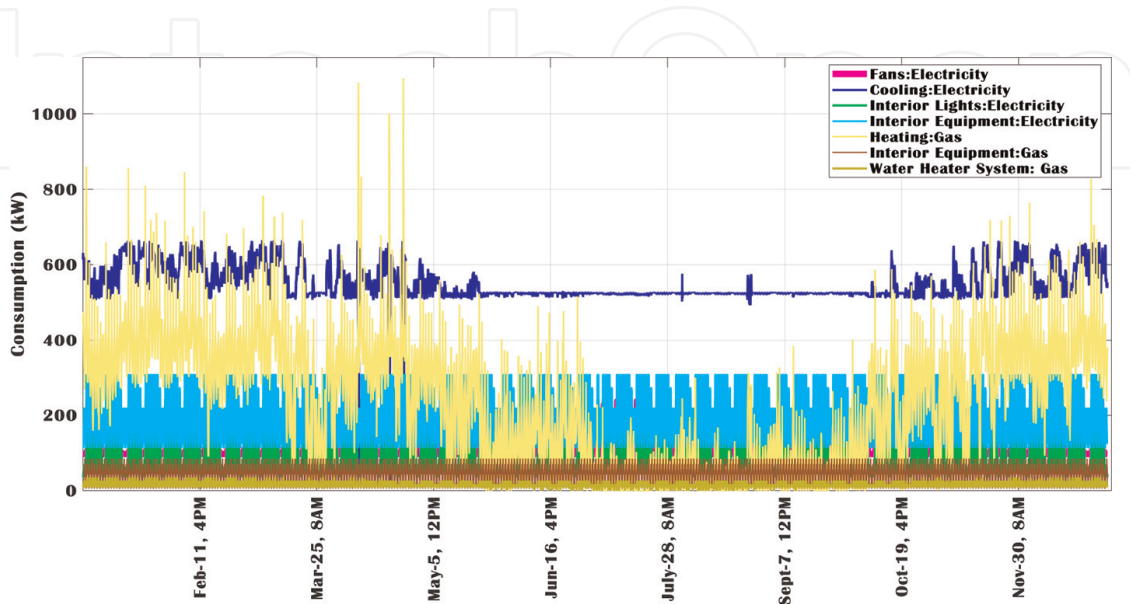


Figure 3.
 Load profile of a Hospital in Miami, Florida for the year 2004.

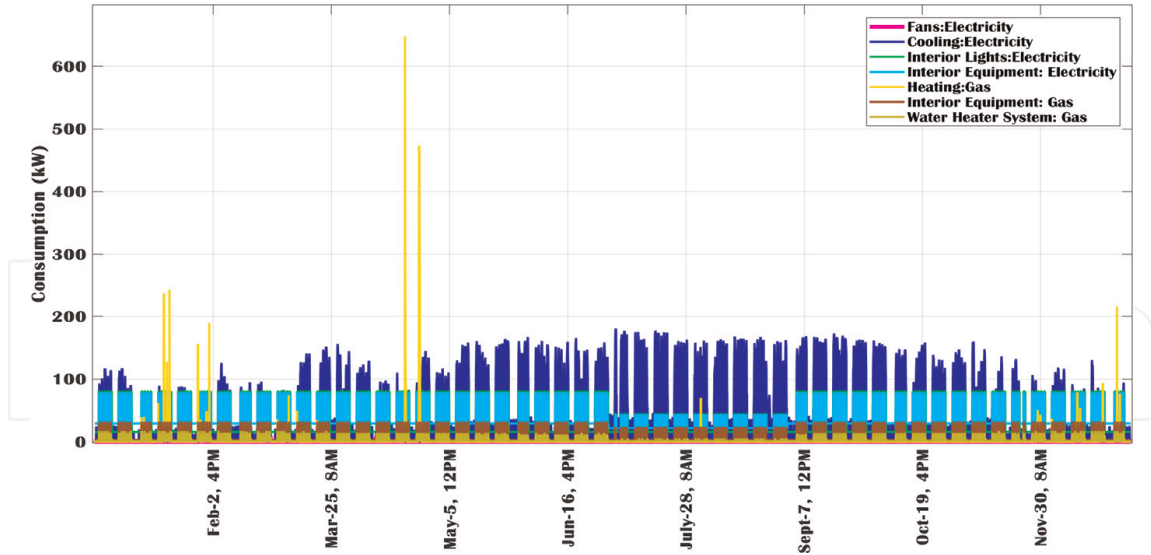


Figure 4.
Load profile of a primary School in Miami, Florida for the year 2004.

methods are shown in Eq. (18) for $E_{max(or\ min)}$ (that is, the corresponding capacity range, in MWh) computation. Load factor is an energy consumption characteristic indicator comparing the actual energy used within a defined period with the energy usage if a peak demand occurs during the same period [121]. Here, the load factor is the ratio of the total yearly consumption and the yearly peak demand in the 365 days' time period for 24 hours/day.

The resulting load factor values for the primary school and hospital are 0.213 and 1.18 respectively. The de-rating factor is the expected deviation in battery parameters under defined conditions. There are no defined de-rating guidelines developed for interconnected batteries as the external controller (or a battery management system) provides the operational set points and limits [122]. Hence, it is assumed that the C-rate is fixed for the battery and the de-rating factor is not taken into consideration. Load growth factor is used to take into account the future facility expansion and corresponding growths in electrical loads that can be handled by the existing energy storage system size. Excess load growths beyond the storage system size addressing capability would need to be independent of the battery and be supplied by a separate feeder or a lateral. In this case, this factor is assumed to be 1, which means that the estimated load growth is twice the existing load.

$$E_{max(or\ min)} = P_b * Operating\ Hours, \quad (18)$$

$$\text{where, } P_b = \frac{\text{Average or Peak Demand (kW) of (Motor + Non - Motor Loads)}}{\text{Load Factor} * \text{De - rating Factor} * \text{Load Growth Factor}},$$

$$\text{Load Factor} = \frac{\text{Total Consumption in a selected period(kWh)}}{\text{Peak Demand(kW)} * \text{Days in the selected period} * \text{Hours/Day in the selected period}},$$

$$\text{Load Growth Factor} = \frac{\text{Estimated Consumption(kWh) in the following year} - \text{Current Yearly Consumption(kWh)}}{\text{Current Yearly Consumption(kWh)}}$$

The sizing is performed under the assumption that gas operated equipment is categorized as motor loads and electricity operated equipment are non-motor loads. This categorization eases the addition (or removal) of a load necessary (or redundant) for the required battery backup or an islanded (off-grid) operation. Additionally, no other renewable sources are taken into consideration, and it is assumed that the battery is connected to the load and the grid, for load demand responses and for battery-specific grid services respectively. The short and long duration grid service responses are taken into account for DOD identification in Section 4. The computed stepwise values and resulting E_{max} and E_{min} are tabulated in **Table 4**. The *Operating Hours* are chosen as 2 and 10 for the minimum (short duration) and maximum (long duration) capacity value computations, respectively. For the primary school, the resulting average energy is 25.735.

MWh, that is the average of the lowest (1.30 MWh) and the highest (50.17 MWh) values. For the hospital, the resulting average energy is 12.445 MWh, which is also the average of the lowest (2.19 MWh) and the highest (22.70 MWh) values. Although the load consumption peaks and frequency of load operations is higher in case of a hospital, the energy storage size requirement for it is comparatively lower than the primary school mainly because of the load factor. Higher is the load factor, lower is the energy storage size requirement, which also results in reduced average per kWh cost.

Further, comparing the load profiles in **Figures 3** and **4**, it can be seen that the peak consumptions take place at the same times of the year for both facilities. Apart from facility occupancy, the external weather plays a major role in this effect. Studies related to this work are out of scope of this chapter and the interested readers are advised to look into papers authored by Sarwat et al. [123, 124]. If the individual equipment current ratings are available, a duty cycle diagram can be built based on the operating periods of the equipment and the corresponding energy requirements can be evaluated [125]. The interconnection topology of the batteries to meet the required battery module size for both EV and RES applications is dependent on the battery management systems performance and application requirements [126].

4. Application-dependent chemistry-specific battery lifecycle performance assessment

Development lifecycle of a battery includes the following phases: material extraction, processing, manufacturing, and assembly, use phase, and end-of-life phase. Assessment of this lifecycle is performed by evaluating the battery chemistry for the intended application using Cradle-to-gate and Cradle-to-grave analysis techniques [4, 9]. The Cradle-to-gate technique covers the upstream and production phases, while the Cradle-to-grave technique includes additional downstream phases, as shown in **Figure 5**. In this study, Cradle-to-gate LCA is performed to identify the energy consumption and environmental impact of a battery chemistry from research and development to commercialization for both an EV and a RES battery. Here, the impact in transportation of batteries is not taken into consideration. The evaluated chemistries are limited to Li-based, Pb-Acid, Ni-MH, Na-S, and VRB. Each chemistry is evaluated for five case studies.

Facility	Sizing Criteria	Motor Loads (Hourly)			Non-Motor Loads (Hourly)				P_b	Corresponding Capacity Range	
		H_g	IE_g	WH_g	F_e	C_e	IL_e	IE_e		Maximum	Minimum
Primary School	Average	6.79	41.14	39.10	39.01	1.20	7.43	3.44	0.65	1.30	6.48
	Peak	31.73	180.71	80.53	79.09	647.88	32.06	17.44	5.02	10.03	50.17
Hospital	Average	112.92	549.86	132.06	207.44	229.23	43.08	14.44	1.10	2.19	10.94
	Peak	238.63	665.70	243.26	310.11	1094.45	84.97	35.34	2.27	4.54	22.7

Hourly Average and Peak values for: H_g : Heating (Gas Operated) (in kW); IE_g : Interior Equipment (Gas Operated) (in kW); WH_g : Water Heater System (Gas Operated) (in kW); F_e : Fans (Electricity Operated) (in kW); C_e : Cooling (Electricity Operated) (in kW); IL_e : Interior Lights (Electricity Operated) (in kW); IE_e : Interior Equipment (Electricity Operated) (in kW); P_b : Battery Power (in MW).

Table 4.
A primary school and a hospital BES capacity sizing based on load profiles in year 2004.

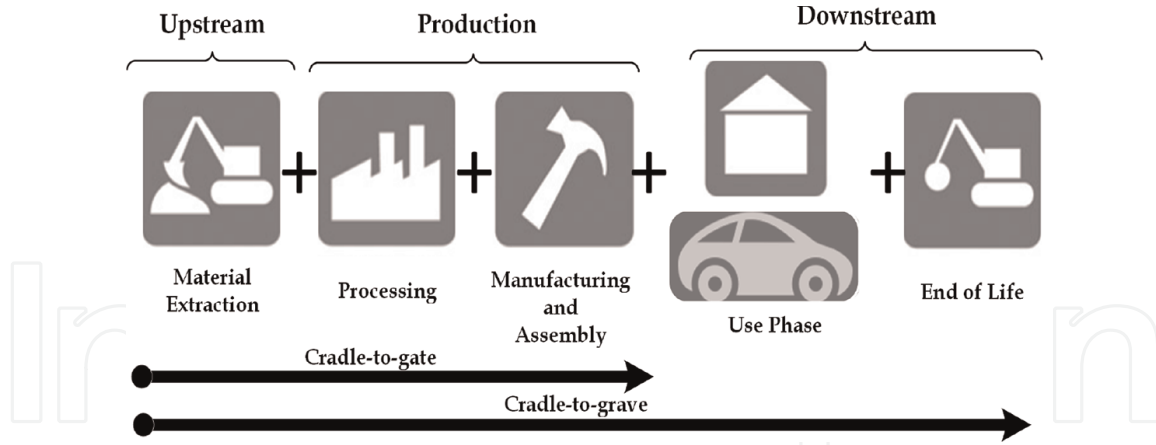


Figure 5.
 RES and EV battery lifecycle phases.

$$C2G/kWh = \frac{C2G/Kg * C_b * m}{E_{life}}, \quad (19)$$

$$\text{where, } C_b = \begin{cases} \frac{10}{\mathcal{L}_{av}}, & \text{if } C_{10} < \mathcal{L}_{10} \\ \frac{C_{10}}{\mathcal{L}_{10}}, & \text{otherwise,} \end{cases}$$

$$m = \frac{E_{res}}{\epsilon_{av}},$$

$$E_{res} = \frac{E_{av}}{\sqrt{\eta_{rt}} * DOD},$$

$$E_{life} = E_{av} * C_{10}$$

Apart from application type categorization, the case studies are majorly divided on the basis of DOD of the battery, which indicate its applicability of operation for the EV or RES application. In RES-based applications, grid services operations are categorized into short (Voltage, Frequency Stability, and Interruption response), medium (Spinning reserve, peak shaving, and contingency reserve), and long duration (load shifting, and energy arbitrage) services [127, 128]. A DOD of 0.2 and 0.8 are selected for short and long duration operations, respectively. For EV storage applications, a medium DOD of 0.5 is selected because of the variation in driving patterns of an EV user, resulting in extreme contrasts (high or low) in consumption from user to user. Case studies use the equations in (19), results for which, along with each parameter's values, are tabulated in **Table 5**. In **Table 5**, the application-specific/–dependent parameters are E_{av} : Average Application Energy (in kWh), C_{10} : Number of cycles demanded by the application in 10 years [129, 130], DOD%: Depth of Discharge %, and E_{life} : Lifetime Energy Delivered (in kWh). The chemistry-specific/–dependent parameters are η_{rt} : Average Round-trip Efficiency [96, 131, 132], ϵ_{av} : Average Specific Energy (in kWh/Kg); \mathcal{L}_{80} : Average Cycle Life of battery at 80% DOD in its lifetime [97, 131, 132], \mathcal{L}_{av} : Average Calendar Life (in Years) [131], C2G/Kg: Cradle-to-gate impact of battery (in KJ/Kg) [133], C_b : Number of batteries used in 10 years' time scale, E_{res} : Resulting System Size (in kWh), m : Battery Mass (in Kg), and C2G/kWh: Cradle-to-gate impact of battery (in KJ/kWh). The E_{av} , C_{10} , DOD%, and E_{life} are the application-specific parameters and η_{rt} , ϵ_{av} , \mathcal{L}_{80} ,

Case study	Application	E_{av}	η_{rt}	ϵ_{av}	Duration	DOD%	L80	C10	Lav	C2G/Kg	Cb	Eres	m	Elife	C2G/kWh	
I	EV storage	105	Li-based	0.86	0.152	Medium	50	10250	450	10	196	1	226.45	1489.8	47250	6.18
			Pb-Acid	0.72	0.04			1250	3	39.6	3.33	247.49	6187.2	17.28		
			Ni-MH	0.8	0.075			600	5	55	2	234.79	3130.5	7.29		
			Na-S	0.75	0.19			3333	13.5	180.7	0.74	242.49	1276.2	3.62		
			VRB	0.68	0.035			13000	15	37.5	0.67	255.60	7303	3.86		
II	RES-primary school	25731	Li-based	0.86	0.152	Long	80	10250	3300	10	196	1	34683.06	228178.05	84912300	0.53
			Pb-Acid	0.72	0.04			1250	3	39.6	3.33	37905.34	947633.57	1.17		
			Ni-MH	0.8	0.075			600	5	55	2	35960.17	479468.88	1.71		
			Na-S	0.75	0.19			3333	13.5	180.7	0.74	37139.50	195471.05	0.31		
			VRB	0.68	0.035			13000	15	37.5	0.67	39148.47	1118527.7	0.33		
III	RES-primary school	25731	Li-based	0.86	0.152	Short	20	10250	3300	10	196	1	138732.25	912712.2	84912300	2.11
			Pb-Acid	0.72	0.04			1250	3	39.6	3.33	151621.37	3790534.3	4.67		
			Ni-MH	0.8	0.075			600	5	55	2	143840.66	1917875.5	6.83		
			Na-S	0.75	0.19			3333	13.5	180.7	0.74	148557	781884.2	1.23		
			VRB	0.68	0.035			13000	15	37.5	0.67	156593.88	4474110.8	1.32		
IV	RES-hospital	12440	Li-based	0.86	0.152	Long	80	10250	3300	10	196	1	16767	110315.8	41052000	0.53
			Pb-Acid	0.72	0.04			1250	3	39.6	3.33	18325.85	458146.3	1.17		
			Ni-MH	0.8	0.075			600	5	55	2	17385.43	231805.7	1.71		
			Na-S	0.75	0.19			3333	13.5	180.7	0.74	17955.59	94503.12	0.31		
			VRB	0.68	0.035			13000	15	37.5	0.67	18926.86	540767.4	0.33		
V	RES-hospital	12440	Li-based	0.86	0.152	Short	20	10250	3300	10	196	1	67071.98	441263.059	41052000	2.11
			Pb-Acid	0.72	0.04			1250	3	39.6	3.33	73303.40	1832585.07	4.67		
			Ni-MH	0.8	0.075			600	5	55	2	69541.71	927222.9	6.83		
			Na-S	0.75	0.19			3333	13.5	180.7	0.74	71822.37	378012.5	1.23		
			VRB	0.68	0.035			13000	15	37.5	0.67	75707.43	2163069.4	1.32		

Table 5.
Selected chemistry-specific LCA of commercialized battery energy storage systems.

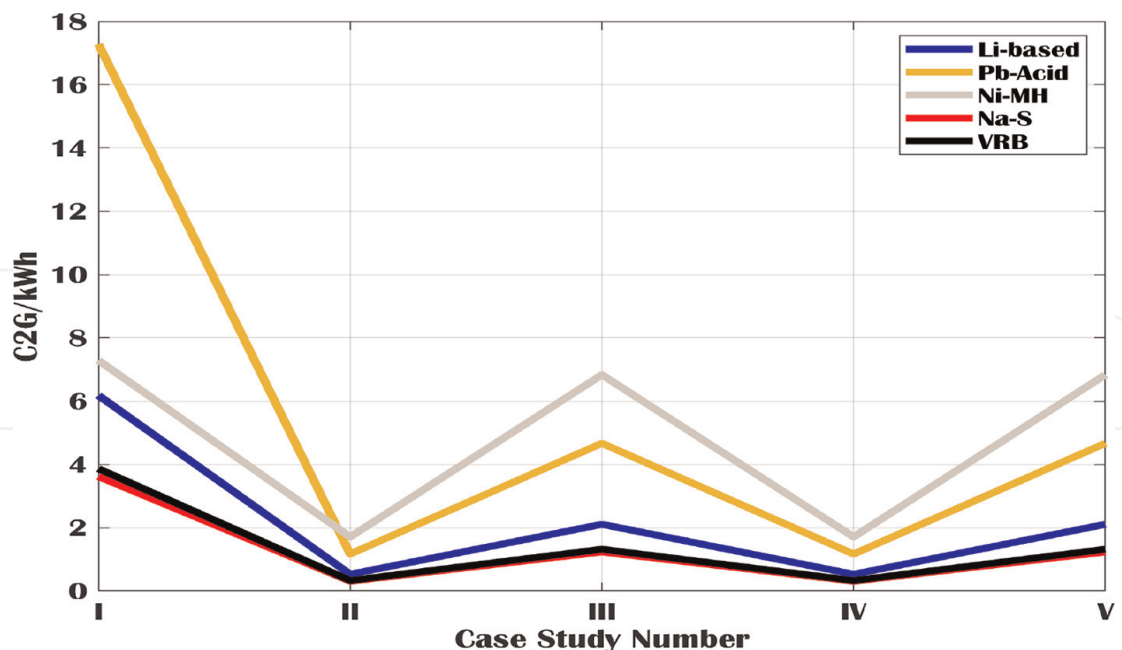


Figure 6. Case study versus cradle-to-gate lifecycle phase impact of selected chemistries.

\mathcal{L}_{av} , C2G/Kg, C_b , E_{res} , m , and C2G/kWh are chemistry-specific parameters. av values are obtained from **Tables 1** and **2**, while E_{av} values are from Sections 3.1 and 3.2. Other parameters are obtained from [97, 129–135].

The resulting Cradle-to-gate lifecycle phase impact of all the chemistries shown in **Figure 6** indicate that the Pb-Acid chemistry has the highest C2G/kWh value for EV applications and Ni-MH has the highest C2G/kWh value for RES applications. Overall, it can also be noticed that the case studies with increased DOD (II and IV) have the lowest impact in the Cradle-to-gate phases.

5. Conclusion and future directions of research

For sized EV storage battery, CED order is: Pb-Acid > Ni-MH > Li-based (6.16 MJ/kWh) > VRB \approx NaS. For sized grid-storage, CED order for: Long duration is: Ni-MH > Pb-Acid > Li-based (0.53 MJ/kWh) \approx VRB \approx NaS and Short duration is: Ni-MH > Pb-Acid > Li-based (2.11 MJ/kWh) > VRB \approx NaS.

Considering the technology readiness level, form factor versatility, other electrochemical factors listed in Section 2.1, and the average C2G impact obtained under all case studies, Li-based chemistries are recommended to be chosen as the favorable chemistry for EV and RES applications. As evident from **Table 6**, the Cradle-to-gate with use system boundary is not commonly analyzed, especially with functional units (as defined by ISO 14040 and 14044) which include both EV and RES applicability. In this figure, Refs. [42, 136–139] have EV's, Refs. [140, 141] have battery chemistry, and Refs. [133, 142–144] have grid storage as respective functional units. Hence, this chapter compensates for this research gap by analyzing both EV and RES functional units, with data obtained from other literatures, in a Cradle-to-gate and use system boundary using CED as the impact category.

The computation approaches discussed in this chapter are simplified for the readers to understand the LCA approach with lucidity. The applicable assumptions

Ref.	Functional Unit*	Data Source(s)			System Boundary			Impact Category*	Conclusion(s)
		E.U. Ecoinvent	U.S. GREET	Other literatures/ battery suppliers	Cradle-to-gate	Cradle-to-gate and use	Cradle-to-grave		
[42]	EV with Li-air battery driven for 1 Km	—	—	✓	—	—	✓	GWP, RD, ET	Environmentally benign cell-level recycling is recommended for future battery developments.
[133]	Li-ion, Pb-acid, NaS, and VRB stationary batteries used to deliver 1 MWh of electricity, for a period of 20 years	✓	—	✓	—	—	✓	GWP, CED, RD, OD, AD, EP, ET, HH	CED order: Pb-acid > NaS > Li-ion ≈ VRB.
[136]	Material production involved in 30 kW, 150 kW, and 160 kW LMO batteries modeled for HEV, PHEV, and EV respectively	—	✓	BatPaC	✓	—	—	GHG	Recycling of specific battery materials can result in energy conservation.
[137]	PHEV using 10 kWh LFP driven for 200,000 Km	✓	—	—	—	✓	—	GWP, RD, OD, PS, EP	In addition to production phase, the environmental impact is expected to be significantly dependent on the relation between the weight of the vehicle and vehicle energy consumption, although there is no data available.
[138]	EV and PHEV using NiMH, LFP, and NMC charged with 50 MJ of energy (≈ 100 Km)	✓	—	—	—	✓	—	GWP, RD, ET, HH, OD, AD	LFP eco-friendlier than NMC. Both of them more eco-friendly than NiMH.
[139]	Volkswagen e-Golf equivalent EV using LMO driven for 24,000 Km, with overall 80% efficiency	✓	—	✓	—	—	✓	GWP, CED, RD	CED is 0.91 MJ/kWh. Use phase and the cell production energy demand are the dominant contributor to the environmental burden.
[140]	LFP and NMC modeled for 1 kWh energy release	✓	—	✓	—	—	✓	GWP, CED, AD, RD	CED order: NMC > LFP.
[141]	26.25 kWh/Kg Al-ion battery production	✓	—	✓	✓	—	—	GWP, RD, OD, AD, EP, ET, HH	Suggests that Al-ion is more a sustainable energy storage source than supercapacitors.

Ref.	Functional Unit*	Data Source(s)			System Boundary			Impact Category*	Conclusion(s)
		E.U. Ecoinvent	U.S. GREET	Other literatures/ battery suppliers	Cradle-to-gate	Cradle-to-gate and use	Cradle-to-grave		
[142]	Advanced Pb-acid, NaS, Li-ion and NaNiCl ₂ used to delivery 1MWh of electricity to the grid	✓	—	✓	—	—	✓	GWP, HH, RD	In terms of environment friendliness, NaNiCl ₂ > NaS > Li-ion > Pb-acid.
[143]	LFP, LTO, LMO, NCA, NMC, NaNiCl ₂ , Pb-Acid, and VRB connected to PV and E.U. grid. Varying sizes.	✓	—	—	—	—	✓	GHG, GWP	Carbon footprint order: Pb-acid > VRB ≈ NaNiCl ₂ > LMO > NMC ≈ NCA > LTO ≈ LFP.
[144]	3.04 MWh/8 MW Li-ion battery model with 1 MW capacity reserve run on 9-bus grid for frequency regulation for 1 year.	—	✓	BatPaC	—	—	✓	GWP, CED, AD	CED order: NMC > NCA > LFP > LMO.
This work	2000Kg EV (105.42 average kWh), Two grid-connected ESS (25.7 and 12.4 MWh) operated for 10 years	—	—	✓	—	✓	—	CED	For sized EV battery, CED order: Pb-Acid > Ni-MH > Li-based (6.16 MJ/kWh) > VRB ≈ NaS For sized grid-storage, CED order: Long duration: Ni-MH > Pb-Acid > Li-based (0.53 MJ/kWh) ≈ VRB ≈ NaS Short duration: Ni-MH > Pb-Acid > Li-based (2.11 MJ/kWh) > VRB ≈ NaS

*GHG: Greenhouse gas emission, HH: Human health, EQ: Ecosystem quality, RD: Resources depletion, CWU: Cumulative water use, GWP: Global warming potential, ET: Ecotoxicity, AD: Acidification, OD: Ozone depletion, PS: Photochemical smog, EP: Eutrophication, CED: Cumulative energy demand; LFP: Lithium iron phosphate, NMC: Lithium nickel manganese cobalt oxide, Li-air: Lithium air, LTO: Lithium-titanium-oxide, LMO: Lithium manganese oxide, NiMH: Nickel metal hydride, Al-ion: Aluminum ion, Pb-Acid: Lead acid, NaS: Sodium sulfur, VRB: Vanadium-redox-flow, NaNiCl₂: Sodium nickel chloride; EV: Electric vehicle, HEV: Hybrid electric vehicle, PHEV: Plug-in hybrid electric vehicle; 80-DOD: 80% DOD selected; GREET: Greenhouse Gases, Regulated Emissions, and Energy Use in Transportation, BatPaC: Argonne National Laboratory's Battery Performance and Cost Model; *: Required parameters, as defined by ISO14040 and ISO14044.*

Table 6.
Comparison of LCA results.

and constraints in both sizing and LCA are mentioned and discussed in their respective sections. Future works can focus on evaluating and sizing additional chemistries for LCA and possible greenhouse gas emissions evaluation. Authors also intend to perform an additional Cradle-to-grave application-dependent chemistry-specific analysis taking other renewable sources into consideration as a part of the future work.

Acknowledgements


The material published is a result of the research supported by the National Science Foundation under the Award number CNS-1553494.

Author details

Arif I. Sarwat*, Asadullah Khalid, Ahmed Hasnain Jalal and Shekhar Bhansali
Department of Electrical and Computer Engineering, Florida International
University, Miami, FL, United States

*Address all correspondence to: asarwat@fiu.edu

IntechOpen

© 2023 The Author(s). Licensee IntechOpen. This chapter is distributed under the terms of the Creative Commons Attribution License (<http://creativecommons.org/licenses/by/3.0>), which permits unrestricted use, distribution, and reproduction in any medium, provided the original work is properly cited. 

References

- [1] Islam A, Domijan A. Weather and reliability, in: IEEE Power Engineering Society General Meeting. 2007;2007:1-5
- [2] Berckmans G, Messagie M, Smekens J, Omar N, Vanhaverbeke L, Van Mierlo J. Cost projection of state-of-the-art lithium-ion batteries for electric vehicles up to 2030. *Energies*. 2017;10:1314
- [3] Mohr M, Peters JF, Baumann M, Weil M. Toward a cell-chemistry specific life cycle assessment of lithium-ion battery recycling processes. *Journal of Industrial Ecology*. 2020;24:1310-1322
- [4] Tolomeo R, De Feo G, Adami R, Sesti Osséo L. Application of life cycle assessment to lithium-ion batteries in the automotive sector. *Sustainability*. 2020;12:4628
- [5] Liu L. Life Cycle Assessment of a Lithium-Ion Battery Pack for Energy Storage Systems: -the Environmental Impact of a Grid-Connected Battery Energy Storage System. [Master's Thesis]. Sweden: Uppsala University, Energy Systems Engineering;; 2020. pp. 1-41
- [6] He X, Kim HC, Wallington TJ, Zhang S, Shen W, De Kleine R, et al. Cradle-to-gate greenhouse gas (ghg) burdens for aluminum and steel production and cradle-to-grave ghg benefits of vehicle lightweighting in China. *Resources, Conservation and Recycling*. 2020;152:104497
- [7] Salgado Delgado MA, Usai L, Ellingsen LA-W, Pan Q, Hammer Strømman A. Comparative life cycle assessment of a novel al-ion and a li-ion battery for stationary applications. *Materials*. 2019;12:3270
- [8] Gouveia J, Mendes A, Monteiro R, Mata T, Caetano N, Martins A. Life cycle assessment of a vanadium flow battery. *Energy Reports*. 2020;6:95-101
- [9] Porzio J, Scown CD. Life-cycle assessment considerations for batteries and battery materials. *Advanced Energy Materials*. 2021;11:2100771
- [10] Stan A-I, Świerczyński M, Stroe D-I, Teodorescu R, Andreasen SJ. Lithium ion battery chemistries from renewable energy storage to automotive and back-up power applications—An overview. In: 2014 International Conference on Optimization of Electrical and Electronic Equipment (OPTIM). Cheia, Romania. New Jersey, USA: IEEE; 2014. pp. 713-720
- [11] Khalid A, Sarwat AI, Fast charging li-ion battery capacity fade prognostic modeling using correlated parameters' decomposition and recurrent wavelet neural network, in: 2021 IEEE Transportation Electrification Conference Expo (ITEC), 2021, pp. 27–32. DOI: 10.1109/ITEC51675.2021.9490177
- [12] Nobili F, Marassi R. Fundamental principles of battery electrochemistry. In: *Batteries: Present and Future Energy Storage Challenges*. Vol. 2. New York, USA: John Wiley & Sons; 2020. pp. 13-48
- [13] Sarwat A, Khalid A, Sundararajan A. Systems and Methods for Forecasting Battery State of Charge. Miami, Florida, USA: United States Patents and Trademarks Office; 2021. pp. 1-38. US Patent 10,969,436
- [14] Khalid A, Sundararajan A, Acharya I, Sarwat A. Prediction of li-ion battery state of charge using multilayer perceptron and long short-term memory models. In: 2019 IEEE Transportation Electrification Conference & Expo. Detroit, Michigan in 2019. New Jersey, USA: IEEE; 2019. pp. 1-6

- [15] Khalid A, Sundararajan A, Sarwat AI. A multi-step predictive model to estimate li-ion state of charge for higher c-rates. In: 2019 IEEE International Conference on Environment and Electrical Engineering and 2019 IEEE Industrial and Commercial Power Systems Europe (EEEIC/I&CPS Europe). Genova, Italy. New Jersey, USA: IEEE; 2019. pp. 1-6
- [16] Khalid A, Sundararajan A, Sarwat A. A statistical out-of-sample forecast to estimate lithiumion parameters that determine state of charge. In: Electrochemical Conference on Energy and the Environment (ECEE 2019): Bioelectrochemistry and Energy Storage. 2019. p. 123021
- [17] Khalid A, Hernandez A, Sundararajan A, Sarwat AI. Simulation-based analysis of equalization algorithms on active balancing battery topologies for electric vehicles. In: Advances in Intelligent Systems and Computing. Vol. 1069. Cham: Springer; 2019. pp. 708-728
- [18] Khalid A, Sundararajan A, Sarwat AI. An Arima-narx model to predict li-ion state of charge for unknown charge/discharge rates. In: 2019 IEEE Transportation Electrification Conference (ITEC-India). Vol. 2019. IEEE. pp. 1-4
- [19] Khalid A, Sarwat AI. Unified univariate-neural network models for lithium-ion battery state-of-charge forecasting using minimized akaike information criterion algorithm. IEEE Access. 2021;9:39154-39170
- [20] Khalid A, Khan M, Stevenson A, Batool S, Sarwat AI. Investigation of cell voltage buffer manipulation attack in a battery management system using unsupervised learning technique. In: 2021 IEEE Design Methodologies Conference (DMC). Detroit, Michigan in 2019. New Jersey, USA: IEEE; 2021. pp. 1-6
- [21] Chen X, Shen W, Vo TT, Cao Z, Kapoor A, An overview of lithium-ion batteries for electric vehicles, In: 2012 10th International Power Energy Conference (IPEC), 2012, Ho Chi Minh City, Vietnam. New Jersey, USA: IEEE; 2012. pp. 230-235. DOI:10.1109/ASSCC.2012.6523269
- [22] Blomgren GE. The development and future of lithium ion batteries. Journal of the Electrochemical Society. 2017;164: A5019-A5025
- [23] Stan A-I, Swierczynski M, Stroe D-I, Teodorescu R, Andreasen S. Lithium ion battery chemistries from renewable energy storage to automotive and back-up power applications — An overview, 2014 international conference on optimization of electrical and electronic equipment. OPTIM. 2014;2014:713-720
- [24] Padmanabh M, Desai MM, Performance and dynamic charge acceptance estimation of different lithium-ion batteries for electric and hybrid electric vehicles, In: 2017 IEEE Transportation Electrification Conference (ITEC-India), Pune, India in 2017. New Jersey, USA: IEEE; 2017. pp. 1-5. DOI: 10.1109/ITEC-India.2017.8333894
- [25] Yoshio M, Brodd RJ, Kozawa A. Lithium-ion Batteries. Vol. 1. New York, USA: Springer-Verlag; 2009
- [26] Yan FJD, Lu L, Ouyang M. Comparing the performances of different energy storage cells for hybrid electric vehicle. In: EVS28 International Electric Vehicle Symposium and Exhibition. Seoul, South Korea: The Korean Society of Automotive Engineers; 2015. pp. 1-13
- [27] Park M, Zhang X, Chung M, Less GB, Sastry AM. A review of conduction

phenomena in li-ion batteries. *Journal of Power Sources*. 2010;**195**:7904-7929

[28] Son J, Park K, Kim H, Chung H. Surface-modification of LiMn_2O_4 with a silver-metal coating. *Journal of Power Sources*. 2004;**126**:182-185

[29] Sun X, Luo X, Zhang Z, Meng F, Yang J. Life cycle assessment of lithium nickel cobalt manganese oxide (ncm) batteries for electric passenger vehicles. *Journal of Cleaner Production*. 2020;**273**:123006

[30] Keil P, Schuster SF, Wilhelm J, Travi J, Hauser A, Karl RC, et al. Calendar aging of lithium-ion batteries: I. impact of the graphite anode on capacity fade. *Journal of the Electrochemical Society*. 2016;**163**:A1872-A1880

[31] Ma J, Wang C, Wroblewski S. Kinetic characteristics of mixed conductive electrodes for lithium ion batteries. *Journal of Power Sources*. 2007;**164**:849-856

[32] Forte F, Pietrantonio M, Pucciarmati S, Puzone M, Fontana D. Lithium iron phosphate batteries recycling: An assessment of current status. *Critical Reviews in Environmental Science and Technology*. 2020;**51**:1-28

[33] Wang C, Hong J. Ionic/electronic conducting characteristics of LiFePO_4 cathode materials: The determining factors for high rate performance. *Electrochemical and Solid-State Letters*. 2007;**10**:A65-A69

[34] Bernardi DM, Go J-Y. Analysis of pulse and relaxation behavior in lithium-ion batteries. *Journal of Power Sources*. 2011;**196**:412-427

[35] Madani SS, Schaltz E, Knudsen Kær S. An electrical equivalent circuit model of a lithium titanate oxide battery. *Batteries*. 2019;**5**:31

[36] Mei J, Cheng EKW, Fong YC. Lithium-titanate battery (lto): A better choice for high current equipment, in: 2016 International Symposium on Electrical Engineering (ISEE). 2016. pp. 1-4. DOI: 10.1109/EENG.2016.7846362.

[37] Zhong Y. *Lithium-Air Batteries: An Overview*. Stanford, CA: Stanford University Courses; 2011. Available from: <http://large.stanford.edu/courses/2011/ph240/zhong2/> [Accessed: April 30, 2020]

[38] Liu T, Vivek JP, Zhao EW, Lei J, Garcia-Araez N, Grey CP. Current challenges and routes forward for nonaqueous lithium-air batteries. *Chemical Reviews*. 2020;**120**:6558-6625

[39] Imanishi N, Yamamoto O. Perspectives and challenges of rechargeable lithium-air batteries. *Materials Today Advances*. 2019;**4**:100031

[40] Lai J, Xing Y, Chen N, Li L, Wu F, Chen R. Electrolytes for rechargeable lithium-air batteries. *Angewandte Chemie International Edition*. 2020;**59**: 2974-2997

[41] Tan P, Jiang H, Zhu X, An L, Jung C, Wu M, et al. Advances and challenges in lithium-air batteries. *Applied Energy*. 2017;**204**:780-806

[42] Zackrisson M, Fransson K, Hildenbrand J, Lampic G, O'Dwyer C. Life cycle assessment of lithium-air battery cells. *Journal of Cleaner Production*. 2016;**135**:299-311

[43] Falconi A. *Electrochemical Li-Ion Battery Modeling for Electric Vehicles [Doctoral Thesis]*. Communauté Université Grenoble ALPES; France: Université Grenoble Alpes; 2017. pp. 1-214

[44] Jeon Y, Noh HK, Song H-K. A lithium-ion battery using partially

lithiated graphite anode and amphiredox LiMn_2O_4 cathode. *Scientific Reports*. 2017;7:14879

[45] Nitta WFLJ, Yushin NG. Li-ion battery materials: Present and future. *Materials Today*. 2015;15:252-264

[46] Karthigeyan V, Aswin M, Priyanka L, Sailesh KND, Palanisamy K. A comparative study of lithium ion (LFP) to lead acid (VRLA) battery for use in telecom power system, In: 2017 International Conference on Computation of Power, Energy Information and Communication (ICCPEIC). 2017. pp. 742-748. DOI: 10.1109/ICCPEIC.2017.8290462

[47] Kam KC, Doeff MM. Electrode materials for lithium ion batteries. *Material Matters*. 2012;7:56-60

[48] Brand M, Gläser S, Geder J, Menacher S, Obpacher S, Jossen A, et al. Quinger, Electrical safety of commercial Li-ion cells based on NMC and NCA technology compared to LFP technology, in: 2013 World Electric Vehicle Symposium and Exhibition (EVS27). 2013. pp. 1-9. DOI: 10.1109/EVS.2013.6914893

[49] Daniel C, Besenhard JO. *Handbook of Battery Materials*. New York, USA: John Wiley & Sons; 2012

[50] Pan J, Li H, Sun H, Zhang Y, Wang L, Liao M, et al. A lithium-air battery stably working at high temperature with high rate performance. *Small*. 2018;14:1703454

[51] Abraham KM, Jiang Z. *Solid Polymer Electrolyte-Based Oxygen Batteries*. Norwood, Massachusetts, USA: United States Patents and Trademarks Office; 1996. pp. 1-9. US Patent 5,510,209.

[52] Liu T, Leskes M, Yu W, Moore AJ, Zhou L, Bayley PM, et al. Cycling Li-O₂

batteries via LiOH formation and decomposition. *Science*. 2015;350:530-533

[53] Liu C, Neale ZG, Cao G. Understanding electrochemical potentials of cathode materials in rechargeable batteries. *Materials Today*. 2016;19:109-123

[54] Sharova V. *Enhancing the Performance of Lithium Batteries through the Development of Improved Electrolyte Formulation, Formation Protocol and Graphite Surface Modification* [Thesis]. Germany: Karlsruher Institut für Technologie (KIT); 2018. DOI: 10.5445/IR/1000079331

[55] Tuller H. Ionic conduction and applications, In: Kasap S, Capper P. editors. *Springer Handbook of Electronic and Photonic Materials*. Springer, Cham: Springer Handbooks; 2007; p. 213. DOI: 10.1007/978-0-387-29185-7_11

[56] Li Q, Chen J, Fan L, Kong X, Lu Y. Progress in electrolytes for rechargeable Li-based batteries and beyond, green. *Energy & Environment*. 2016;1:18-42

[57] Wang SLHSSQY, Kadam A. Review on modeling of the anode solid electrolyte interphase (SEI) for lithium-ion batteries. *npj Computational Materials*. Vol. 4. USA: Nature Publishing Group; 2018. pp. 1-26

[58] Ekström H, Lindbergh G. A model for predicting capacity fade due to SEI formation in a commercial graphite/LiFePO₄ cell. *Journal of the Electrochemical Society*. 2015;162:A1003-A1007

[59] Ramakrishnan S, Venugopalan S, Jeyakumar AE. Prediction of retained capacity and EODV of Li-ion batteries in LEO spacecraft batteries. arXiv

Computing Research Repository. 2010;2: 128-132. Available from: <http://arxiv.org/abs/1004.4480>

[60] Kellner Q, Hosseinzadeh E, Chouchelamane G, Widanage WD, Marco J. Battery cycle life test development for high-performance electric vehicle applications. *Journal of Energy Storage*. 2018;15:228-244

[61] Kravchyk KV, Bhauriyal P, Piveteau L, Guntlin CP, Pathak B, Kovalenko MV. High-energy-density dual-ion battery for stationary storage of electricity using concentrated potassium fluorosulfonylimide. *Nature Communications*. 2018;9:1-9

[62] Will F. Assessment of research needs for advanced battery systems. In: Report of the Committee on Battery Materials Technology. Washington, D.C., USA: National Research Council (U.S.), National Academy Press; 1982. pp. 1-183

[63] Gandhi KS. Modeling of sulfation in a flooded lead-acid battery and prediction of its cycle life. *Journal of the Electrochemical Society*. 2020;167:013538

[64] May GJ, Davidson A, Monahov B. Lead batteries for utility energy storage: A review. *Journal of Energy Storage*. 2018;15:145-157

[65] Hong B, Yu X, Jiang L, Xue H, Liu F, Li J, et al. Hydrogen evolution inhibition with diethylenetriamine modification of activated carbon for a lead-acid battery. *RSC Advances*. 2014;4:33574-33577

[66] Sugumaran N, Everill P, Swogger SW, Dubey D. Lead acid battery performance and cycle life increased through addition of discrete carbon nanotubes to both electrodes. *Journal of Power Sources*. 2015;279:281-293

[67] Lee CH, Lee SU. Theoretical basis of electrocatalysis. In: *Electrocatalysts for Fuel Cells and Hydrogen Evolution-Theory to Design*. London, UK: IntechOpen; 2018. p. 13

[68] Albright G, Edie J, Al-Hallaj S. A Comparison of Lead Acid to Lithium-Ion in Stationary Storage Applications. *Alternative Energy eMagazine Industry*; 2012

[69] Nadeem F, Hussain SMS, Tiwari PK, Goswami AK, Ustun TS. Comparative review of energy storage systems, their roles, and impacts on future power systems. *IEEE Access*. 2019;7:4555-4585

[70] Liang Y, Zhao C-Z, Yuan H, Chen Y, Zhang W, Huang J-Q, et al. A review of rechargeable batteries for portable electronic devices. *InfoMat*. 2019;1:6-32

[71] Vega-Garita V, Hanif A, Narayan N, Ramirez-Elizondo L, Bauer P. Selecting a suitable battery technology for the photovoltaic battery integrated module. *Journal of Power Sources*. 2019;438: 227011

[72] Xu X, Zhou D, Qin X, Lin K, Kang F, Li B, et al. A room-temperature sodium-sulfur battery with high capacity and stable cycling performance. *Nature Communications*. 2018;9:1-12

[73] Fan X, Liu B, Liu J, Ding J, Han X, Deng Y, et al. Battery technologies for grid-level large-scale electrical energy storage. *Transactions of Tianjin University*. 2020;26:1-12

[74] Zahrul F, Lee W, Mohd F, Amir B. Modeling of sodium sulfur battery for power system applications. *Journal of ELEKTRIKA*. 2007;9:66-72

[75] Capasso C, Veneri O. Laboratory bench to test zebra battery plus super-capacitor based propulsion systems for

urban electric transportation. *Energy Procedia*. 2015;75:1956-1961

[76] Revankar ST. Chapter six - chemical energy storage. In: Bindra H, Revankar S, editors. *Storage and Hybridization of Nuclear Energy*. London, UK: Academic Press; 2019. pp. 177-227

[77] Frutschy K, Chatwin T, Bull R. Cell overcharge testing inside sodium metal halide battery. *Journal of Power Sources*. 2015;291:117-125

[78] Galloway RC, Haslam S. The zebra electric vehicle battery: Power and energy improvements. *Journal of Power Sources*. 1999;80:164-170

[79] Sakaebe H. *ZEBRA Batteries*, Springer New York, New York, NY: Springer; 2014. pp. 2165–2169. DOI: 10.1007/978-1-4419-6996-5_437

[80] Brady M et al. *Assessment of Battery Technology for Rail Propulsion Application*, Technical Report. United States: Federal Railroad Administration; 2017

[81] Elia GA, Kravchyk KV, Kovalenko MV, Chacón J, Holland A, Wills RG. An overview and prospective on al and al-ion battery technologies. *Journal of Power Sources*. 2021;481:228870

[82] Yuan D, Zhao J, Manalastas W, Kumar S, Srinivasan M. Emerging rechargeable aqueous aluminum ion battery: Status, challenges, and outlooks. *Nano Materials Science*. 2019;2:248-263

[83] Lin M-C, Gong M, Lu B, Wu Y, Wang D-Y, Guan M, et al. An ultrafast rechargeable aluminium-ion battery. *Nature*. 2015;520:324-328

[84] Li C, Hou C-C, Chen L, Kaskel S, Xu Q. Rechargeable al-ion batteries. *EnergyChem*. 2020;3:100049

[85] Wang P, Chen Z, Ji Z, Feng Y, Wang J, Liu J, et al. A flexible aqueous al ion rechargeable full battery. *Chemical Engineering Journal*. 2019;373: 580-586

[86] Kim H-T, Lee J-H, Kim DS, Yang JH. Redox flow-zn-br. In: *Batteries: Present and Future Energy Storage Challenges*. Vol. 2. New York, USA: Wiley; 2020. pp. 230-235, 311

[87] Biswas S, Senju A, Mohr R, Hodson T, Karthikeyan N, Knehr KW, et al. Minimal architecture zinc-bromine battery for low cost electrochemical energy storage. *Energy & Environmental Science*. 2017;10:114-120

[88] Lazard L. Lazard's levelized cost of storage analysis, version 1.0. 2015. Available from: <https://www.lazard.com/media/450774/lazards-levelized-cost-of-storage-version-40-vfinal.pdf>

[89] Butler PC, Eidler PA, Grimes PG, Klassen SE, Miles RC. Zinc/bromine batteries. In: *Handbook of Batteries*. USA: Mc-Graw-Hill; 2001. pp. 1-22

[90] Weaver JF. 'world's smallest' zinc bromine residential flow batteries coming for lithium, November 2017. Available from: <https://electrek.co/2017/11/06/zinc-bromine-batteries-coming-for-lithium/>

[91] Christensen R. Vanadium redox flow battery. In: *Technology Data for Energy Storage*: November 2018. København, Denmark: Danish Energy Agency; 2018. pp. 113-146

[92] Molina MG. Energy storage and power electronics technologies: A strong combination to empower the transformation to the smart grid. *Proceedings of the IEEE*. 2017;105: 2191-2219

- [93] Council NR et al. Reducing the Fuel Consumption and Greenhouse Gas Emissions of Medium-and Heavy-Duty Vehicles, Phase Two: First Report. National Academies Press; 2014
- [94] Gao D, Jiang D, Liu P, Li Z, Hu S, Xu H. An integrated energy storage system based on hydrogen storage: Process configuration and case studies with wind power. *Energy*. 2014;**66**:332-341
- [95] Sato Y, Takeuchi S, Kobayakawa K. Cause of the memory effect observed in alkaline secondary batteries using nickel electrode. *Journal of Power Sources*. 2001;**93**:20-24
- [96] Letcher TM, editor. Chapter 24 - storing energy in China—An overview. In: *Storing Energy*. Oxford: Elsevier; 2016. pp. 509-527
- [97] Akinyele D, Belikov J, Levron Y. Battery storage technologies for electrical applications: Impact in stand-alone photovoltaic systems. *Energies*. 2017;**10**:1760
- [98] Wesoff E. Exploding sodium sulfur batteries from ngk energy storage. 2011. Available from: <https://www.greentechmedia.com/articles/read/Exploding-Sodium-Sulfur-Batteries-From-NGK-Energy-Storage>
- [99] Wesoff E. Battery room fire at kahuku wind-energy storage farm. 2012. Available from: <https://www.greentechmedia.com/articles/read/Battery-Room-Fire-at-Kahuku-Wind-Energy-Storage-Farm>
- [100] Ha S, Kim J-K, Choi A, Kim Y, Lee KT. Sodium–metal halide and sodium–air batteries. *ChemPhysChem*. 2014;**15**: 1971-1982
- [101] Parkhideh B. Storage technologies for hybrid electric buses, zebra battery. 2006. Available from: https://www.euromatic.no/ZEBRA_Aug17.pdf
- [102] Yu J, Hu Y-S, Pan F, Zhang Z, Wang Q, Li H, et al. A class of liquid anode for rechargeable batteries with ultralong cycle life. *Nature Communications*. 2017;**8**:1-7
- [103] Li G, Chang H, Lu X, Sprenkle V. Low cost and reliable sodium-metal halide (na-mh) batteries for stationary energy storage application, *TechConnect. Briefs*. 2017;**2**:122-125
- [104] Levy NR, Ein-Eli Y. Aluminum-ion battery technology: A rising star or a devastating fall? *Journal of Solid State Electrochemistry*. 2020;**24**:1-5
- [105] Leisegang T, Meutzner F, Zschornak M, Münchgesang W, Schmid R, Nestler T, et al. The aluminum-ion battery: A sustainable and seminal concept? *Frontiers in Chemistry*. 2019;**7**:268
- [106] Chen R, Kim S, Chang Z. Redox flow batteries: Fundamentals and applications. In: *Redox: Principles and Advance Applications*. 2017. pp. 103-118
- [107] Conca J. Energy's future - battery and storage technologies. New York, USA: Forbes; 2019. Available from: <https://www.forbes.com/sites/jamesconca/2019/08/26/energys-future-battery-and-storage-technologies/#428d111544cf>
- [108] Xie X. Vanadium Redox-Flow Battery. Stanford, CA: Stanford University Courses; 2017
- [109] B.-Z. Magnes, I. B. David, E. Lancry, M. Bergstein-Freiberg, Additives for Zinc-Bromine Membraneless Flow Cells, 2017. US Patent 9,722,272.

- [110] Rajarathnam GP, Vassallo AM. Description of the zn/br rfb system. In: *The Zinc/Bromine Flow Battery: Materials, Challenges, and Practical Solutions for Technology Advancement*. Singapore: Springer; 2016. pp. 11-28
- [111] Gao DEA. Vanadium redox flow batteries. In: *Storing Energy: With Special Reference to Renewable Energy Sources*. Amsterdam, Netherlands: Elsevier; 2016. pp. 227-248
- [112] Leahy MJ, Connolly D, Buckley DN. Wind energy storage technologies. In: *Wind Power Generation and Wind Turbine Design*. WIT Press; 2010. pp. 661-714
- [113] Pang Z, Gong Y, Yuan M, Li X. A newly designed modular znbr₂ single cell structure. In: *Batteries*. Vol. 6. Basel, Switzerland: MDPI; 2020. p. 27
- [114] Khalid A, Sundararajan A, Hernandez A, Sarwat A. Facts approach to address cybersecurity issues in electric vehicle battery systems. In: *2019 IEEE Technology & Engineering Management Conference (TEMSCON)*. 2019
- [115] Huzayyin OA, Salem H, Hassan MA. A representative urban driving cycle for passenger vehicles to estimate fuel consumption and emission rates under real-world driving conditions. *Urban Climate*. 2021;**36**:100810
- [116] USEPA. Vehicle and fuel emissions testing: Dynamometer drive schedules. 2017. Available from: <http://www.epa.gov/vehicle-and-fuel-emissions-testing/dynamometer-drive-schedules>
- [117] Eaton, Technical data td00405018e: Generator sizing guide, 2009.
- [118] Althouse JR, Surbrook TC. *Electrical Tech Note — 600: Standby Power Systems*, 2008
- [119] Wilcox S, Marion W. Users manual for tmy3 data sets, national renewable energy laboratory technical report nrel/tp-581-43156, Golden, Colorado: National Renewable Energy Laboratory; Available from: <https://www.nrel.gov/docs/fy08osti/43156.pdf> [Accessed: July, 2020]
- [120] Office of Energy Efficiency & Renewable Energy (EERE). *Commercial and Residential Hourly Load Profiles for all tmy3 Locations in the United States*. EERE; 2013
- [121] A. Energy, understanding load factor. Available from: <https://austinenergy.com/wcm/connect/8fe76160-0f73-4c44-a735-529e5c7bee61/understandingLoadFactor.pdf?MOD=AJPERES&CVID=kC1aR-I> [Accessed: July 2020]
- [122] Sun Y, Saxena S, Pecht M. Derating guidelines for lithium-ion batteries. *Energies*. 2018;**11**:3295
- [123] Sarwat AI, Domijan A, Amini MH, Damnjanovic A, Moghadasi A. Smart grid reliability assessment utilizing boolean driven markov process and variable weather conditions, in. *North American Power Symposium (NAPS)*. 2015;**2015**:1-6
- [124] Sarwat AI, Amini M, Domijan A, Damnjanovic A, Kaleem F. Weather-based interruption prediction in the smart grid utilizing chronological data, *journal of modern power systems and clean. Energy*. 2016;**4**:308-315
- [125] Webb K. Section 6: Battery bank sizing procedures, ese 471 – energy storage systems. 2019. Available from: http://web.engr.oregonstate.edu/~webbky/ESE471_files/Section%206%20Battery%20Sizing.pdf
- [126] Khalid A, Sarwat AI. Battery module performance analysis under

varying interconnection topology for electric vehicles. In: 2019 IEEE Transportation Electrification Conference (ITEC-India). 2019. pp. 1-5

[127] Leadbetter J. Residential Battery Energy Storage Systems for Renewable Energy Integration and Peak Shaving [Master's Thesis]. Halifax, Canada: Dalhousie University; 2012. pp. 1-148

[128] Sanfiel JJ, Khalid A, Parvez I, Sarwat AI. Simulation-based sizing and impact study of microgrid on a university campus. In: Southeast con 2021. IEEE; 2021. pp. 1-8

[129] Yang F, Xie Y, Deng Y, Yuan C. Predictive modeling of battery degradation and greenhouse gas emissions from us state-level electric vehicle operation. Vol 9. London, UK: Nature Communications; 2018. pp. 1-10

[130] Fqx S. How Does Depth of Discharge Factor into Grid Connected Battery Systems? 2013

[131] Mongird K, Viswanathan VV, Balducci PJ, Alam MJE, Fotedar V, Koritarov VS, et al. Energy storage technology and cost characterization report. In: Technical Report. Richland, WA (United States): Pacific Northwest National Lab. (PNNL); Richmond, Washington, USA: Pacific Northwest National Lab; 2019

[132] Rydh CJ, Sandén BA. Energy analysis of batteries in photovoltaic systems. part i: Performance and energy requirements. Energy Conversion and Management. 2005;46:1957-1979

[133] Hiremath M, Derendorf K, Vogt T. Comparative life cycle assessment of battery storage systems for stationary applications. Environmental Science & Technology. 2015;49:4825-4833

[134] Bourgeois R. Sodium-metal halide batteries for stationary applications. In: Proc. 2010 Battcon Station. Battery Conf. Orlando. Pompano Beach, FL: Battcon/Albercorp; 2010. pp. 11-16

[135] Rantik M et al, Life Cycle Assessment of Five Batteries for Electric Vehicles under Different Charging Regimes, KFB. 1999

[136] Dunn JB, Gaines L, Sullivan J, Wang MQ. Impact of recycling on cradle-to-gate energy consumption and greenhouse gas emissions of automotive lithium-ion batteries. Environmental Science & Technology. 2012;46:12704-12710

[137] Zackrisson M, Avellán L, Orlenius J. Life cycle assessment of lithium-ion batteries for plug-in hybrid electric vehicles—critical issues. Journal of Cleaner Production. 2010;18:1519-1529

[138] Majeau-Bettez G, Hawkins TR, Strømman AH. Life cycle environmental assessment of lithiumion and nickel metal hydride batteries for plug-in hybrid and battery electric vehicles. Environmental Science & Technology. 2011;45:4548-4554

[139] Notter DA, Gauch M, Widmer R, Wager P, Stamp A, Zah R, et al. Contribution of li-ion batteries to the environmental impact of electric vehicles. Environ. Sci. Technol. 2010;44:6550-6556

[140] Jachura A, Sekret R. Life cycle assessment of the use of phase change material in an evacuated solar tube collector. Energies. 2021;14:4146

[141] Melzack N, Wills R, Cruden A, et al. Cleaner energy storage: Cradle-to-gate lifecycle assessment of aluminium-ion batteries with an aqueous electrolyte.

Frontiers in Energy Research. 2021;**9**:
699919

[142] Oliveira L, Messagie M, Mertens J, Laget H, Coosemans T, Van Mierlo J. Environmental performance of electricity storage systems for grid applications, a life cycle approach. Energy Conversion and Management. 2015;**101**:326-335

[143] Baumann M, Peters J, Weil M, Grunwald A. Co2 footprint and life-cycle costs of electrochemical energy storage for stationary grid applications. Energy Technology. 2017;**5**:1071-1083

[144] Ryan NA, Lin Y, Mitchell-Ward N, Mathieu JL, Johnson JX. Use-phase drives lithium-ion battery life cycle environmental impacts when used for frequency regulation. Environmental Science & Technology. 2018;**52**:10163-10174